Available online at www.sciencedirect.com
ScienceDirect
Journal of Nuclear Materials 376 (2008) 60–65
journal of nuclear materials
www.elsevier.com/locate/jnucmat

Isotope effects in thermal neutron transmission and backscattering processes for ε-phase zirconium hydrides and deuterides

B. Tsuchiya [a,*], R. Yasuda [b], M. Teshigawara [b], K. Konashi [a], S. Nagata [a], T. Shikama [a], M. Yamawaki [c]

[a] Institute for Materials Research, Tohoku University, 2-1-1, Katahira, Aoba-ku, Sendai 980-8577, Japan
[b] Tokai Research Establishment, Japan Atomic Energy Agency, Tokai-mura, Ibaraki-ken 319-1195, Japan
[c] Department of Applied Physics, Graduate School of Engineering, Tokai University, 1117, Kitakaname, Hiratsuka, Kanagawa 259-1292, Japan

Received 9 May 2007; accepted 30 December 2007

Abstract

Distributions of hydrogen isotope concentrations in ε-phase zirconium hydrides and deuterides (ε-ZrH_x and ε-ZrD_x: $1.8 < x < 2.0$) were investigated by neutron radiography (NRG). The NRG images of the thermal neutron transmission and backscattering revealed hydrogen concentration dependence and isotope differences. The thermal neutron mass attenuation coefficients in relation to the hydrogen isotope concentrations were determined from the transmission NRG images. The results showed the isotope effects of the thermal neutron mass attenuation coefficients for ε-ZrH_x to be about 6–9 times higher than those for ε-ZrD_x. The neutron scattering processes for transmission and backscattering NRG images of ε-ZrH_x and ε-ZrD_x were also analyzed using a general Monte Carlo neutron-particle transport (MCNP) code.
© 2008 Elsevier B.V. All rights reserved.

PACS: 25.60.Bx; 28.20.Cz

1. Introduction

New irradiation targets including ε-phase zirconium hydrides or deuterides of which the ratio of protium (or deuterium) to zirconium (H/Zr or D/Zr) is over 1.7 have been developed with the aim of transmuting actinide radioactive wastes. The actinide hydride target assemblies are loaded in the core region of fast reactors containing mixed oxide fuels [1]. Large amounts of hydrogen isotope atoms in zirconium hydrides or deuterides can play a major neutron-moderating role. During reactor irradiation, a temperature gradient develops radially in the target, and the hydrogen atoms migrate to the lower-temperature target surface by thermal diffusion [2]. A small change of hydrogen concentration has a large influence on thermal, electrical and mechanical properties, due to changes in charge density between Zr and H atoms [3,4]. For example, the hydrogen concentration dependence of the thermal conductivity σ, electrical resistivity ρ and Vickers microhardness H_v for the ε-phase zirconium hydrides at 300 K were $\sigma = 24.4$–82.1 W/m K (H/Zr = D/Zr = 1.76–1.99) [5], $\rho = 54.7 \times 10^{-2}$–$24.7 \times 10^{-2}\ \Omega$ m (H/Zr = D/Zr = 1.81–1.96) [6] and $H_v = 155 \pm 12$–164 ± 10 (H/Zr = 1.7–2.0) [7], respectively. The change in some properties caused by the hydrogen concentration gradient inside the hydride targets induces the production of defects, such as cracks and splits that lead to a reduction in lifetime. It is essential to evaluate the redistribution of the hydrogen concentration in the target as a function of neutron fluence and temperature. Recently, there have been some reports related to the quantitative evaluations concerning the spatial distribution of hydrogen within metals using a neutron radiography (NRG) technique employed as a non-destructive hydrogen analysis for post-irradiation examination (PIE) experiments [8–10]. However, there are no reports related to

* Corresponding author. Tel.: +81 22 215 2063; fax: +81 22 215 2061.
E-mail address: tsuchiya@imr.tohoku.ac.jp (B. Tsuchiya).

0022-3115/$ - see front matter © 2008 Elsevier B.V. All rights reserved.
doi:10.1016/j.jnucmat.2007.12.008

NRG data for the high concentration of hydrogen isotopes in ε-phase zirconium hydrides and deuterides with non-stoichiometric structures. In addition, an estimation method for hydrogen redistribution using NRG data is not yet fully established.

In the present study, the distributions of different hydrogen isotope concentrations in near-stoichiometric ε-phase zirconium hydrides and deuterides were observed using NRG with thermal neutron transmission and backscattering processes. The thermal neutron linear attenuation coefficients were estimated using empirical equations as a function of hydrogen concentration, obtained from the transmission NRG images. The interactions of thermal neutrons with hydrogen isotope atoms in the hydrides and deuterides were also analyzed using a general Monte Carlo neutron-particle transport (MCNP) code [11].

2. Experiments

2.1. Preparation of zirconium hydrides and deuterides

Non-stoichiometric zirconium hydrides and deuterides ($ZrH_{1.83}$, $ZrH_{1.91}$, $ZrH_{1.99}$, $ZrD_{1.82}$, $ZrD_{1.92}$ and $ZrD_{1.98}$) specimens were prepared using a Sieverts apparatus. Zirconium pure metal (99.8% quality), about 10 mm in diameter and about 1 mm in thickness, was heated at 1073 K for 1 h in a quartz tube that had been evacuated to 4.0×10^{-5} Pa. They were then exposed to pure protium or deuterium gas, which had been passed through a gas line cooled with liquid nitrogen to remove water, in the quartz tube at pressures ranging from 0.1 to 1.0×10^{5} Pa for 4 h. The annealing temperature was then reduced to room temperature at a rate of 8.7×10^{-3} K/s, keeping the sample in the tube. The compositions of the specimens were measured based on hydrogen pressure changes when the equilibrium was achieved at 1073 K, mass gains before and after hydrogenation, and X-ray diffraction (XRD) patterns at room temperature [12]. The estimated values of the compositions showed little difference, all being within about ±2.5%. Ultimately, the composition as calculated from the mass gain was chosen, since the hydrogen gases were kept in the tube down to room temperature. In the case of deuterium absorption, there was a slight risk that traces of residual protium or water in the deuterium gas had been absorbed during the hydrogenation, with the result that pure deuterides with exact compositions would not be fabricated. Our group confirmed, however, using an elastic recoil detection (ERD) technique, that there were no protium atoms inside the deuteride specimens. The measurements of hydrogen isotope contributions in hydrides and deuterides using the ERD technique were performed using a 2.8 MeV He^{2+} ion probe beam from a Tandem accelerator, installed at Tohoku University's Institute for Materials Research. It is possible to distinguish protium and deuterium atoms with different masses by elastic collision with He^{2+} ions [10]. The XRD measurements also confirmed that the zirconium–hydrogen isotopes system at room temperature consists of the ε-phase only with tetragonal distortion.

2.2. Simultaneous thermal neutron transmission and backscattering measurements by NRG

The NRG measurements were performed at the 2nd thermal neutron radiography facility (TNRF-2), installed in JRR-3M at the Japan atomic energy agency (JAEA). A schematic of simultaneous thermal neutron transmission and backscattering measurements using the NRG technique is shown in Fig. 1. The ZrH_x and ZrD_x specimens were directly fixed to the surface of an aluminum (Al) cassette with Al tape and irradiated at a thermal neutron flux of 1.2×10^{12} n/m^2/s at room temperature. The exposure time for each specimen was 4 s. The transmitted or backscattered neutrons were detected by imaging plates [13] in the Al cassettes which were set up in front and behind the specimens, respectively. In the imaging plate, neutron converter compounds such as gadolinium (Gd) were uniformly dispersed in photostimulated luminescence (PSL) material consisting of BaF (Br, I):Eu^{2+}. The imaging plate was imaged by an imaging plate reader (BAS-2000) with a reading resolution of 100 μm × 100 μm. The image analysis processing was conducted using imaging plate lab software on a personal computer.

3. Experimental results and discussion

3.1. NRG images from forward-scattered and back-scattered neutrons

Typical neutron transmitted and backscattered images of $ZrH_{1.91}$ (or $ZrD_{1.92}$) are shown in Fig. 2(a), (c) and (b), (d), respectively. The isotope effect can be clearly observed for the thermal neutron scattering process, as compared with Fig. 2(a) and (b) and Fig. 2(c) and (d). For the transmission images in Fig. 2(a) and (b), the brightness at the edge of the inside area is darker than at the center, while that around the specimen is a little lighter than the background.

Fig. 3(a)–(d) show transverse line profiles which cross the center of the images in Fig. 2(a)–(d). The vertical axis is ΔPSL (=PSL_{image}/PSL_{bg}) value, where PSL_{image} and

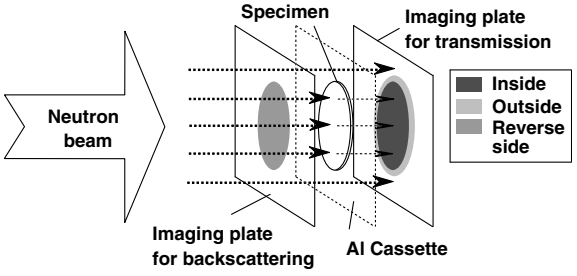

Fig. 1. Schematic of simultaneous measurements for neutron transmission and backscattering by NRG.

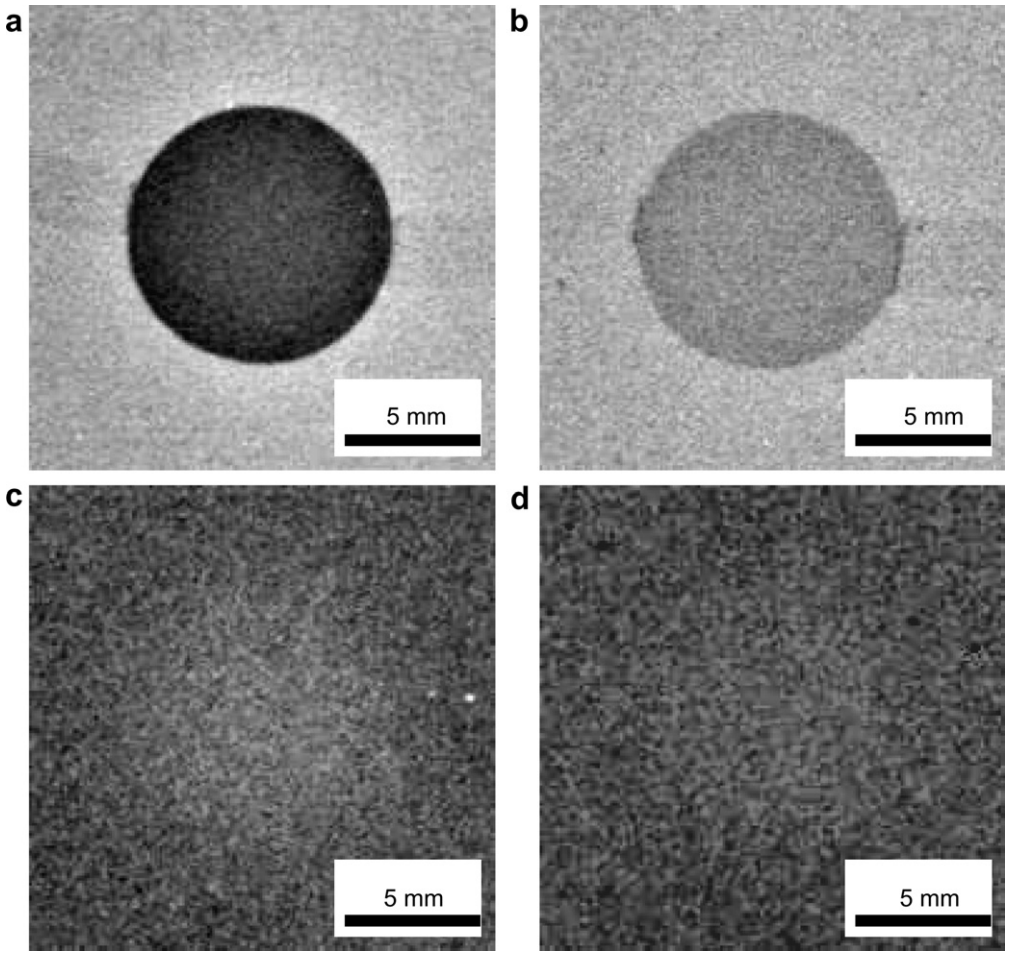

Fig. 2. NRG images of thermal neutron transmission ((a) $ZrH_{1.91}$ and (b) $ZrD_{1.92}$) and backscattering ((c) $ZrH_{1.91}$ and (d) $ZrD_{1.92}$).

PSL_{bg} represent numerical values of PSL on the imaging plate with and without the specimen (the background), respectively, and t is specimen thickness. In Fig. 3(a) and (b), the ΔPSL value at the center of the inside area is clearly higher that at the edge, and that around the specimen is higher than the background. The isotope differences in the neutron transmission and backscattering NRG images are also clearly evident. The mean ΔPSL values at several points inside, outside and on the reverse side are summarized with an error of ±2%, obtained from the scattered data, for various H/Zr and D/Zr ratios in Fig. 4(a) and (b), respectively. The inside and outside are distinguished by an area of 10.0 mm in diameter and 10.0–10.5 mm in diameter, respectively, in the transmission NRG image. The part of the reverse side represents the area of 10.0 mm in diameter in the backscattering NRG image. The ΔPSL values for Zr (H/Zr = D/Zr = 0) are also plotted in Fig. 4(a) and (b) for comparison with the results for the hydrides and deuterides. The mean inside ΔPSL values of ZrH_x decrease with increasing hydrogen concentration, whereas the mean outside and reverse side ΔPSL values increase. However, it is not possible to evaluate the hydrogen distribution from the neutron backscattering image. In ZrD_x, the hydrogen concentration dependence is not clearly observed, since the average elastic and capture cross sections for deuterium in thermal neutron flux with a Maxwellian distribution at 0.0253 eV are 3.389 and 4.876×10^{-4} barn, much lower than the 20.78 and 0.2943 barn for protium and 10.59 and 1.106 barn for zirconium [14]. It was also found that the mean ΔPSL value of Zr for transmission fell between those of ZrH_x and ZrD_x. This may be caused by the difference between the density of Zr metal and deuterides, and a trace of residual protium (H/Zr < 0.2) as interstitial atoms in the hexagonal structure of Zr and no presence of protium in deuterides, according to the results of hydrogen analysis using ERD.

3.2. Evaluation of thermal neutron mass attenuation coefficients for ε-ZrH_x and ε-ZrD_x

Since the specimen thickness is below 1 mm, the multi-scattering of thermal neutrons with hydrogen atoms in the hydride and deuteride can be ignored by taking into account the mean free path of about 6.8 mm, where the average elastic cross section for protium in thermal neutron flux with a Maxwellian distribution at 0.0253 eV is 20.78 barn [14] and the density of $ZrH_{2.0}$ is 5.574×10^{-3} g/mm^3 [15]. The neutron scattering and absorption due to interaction with

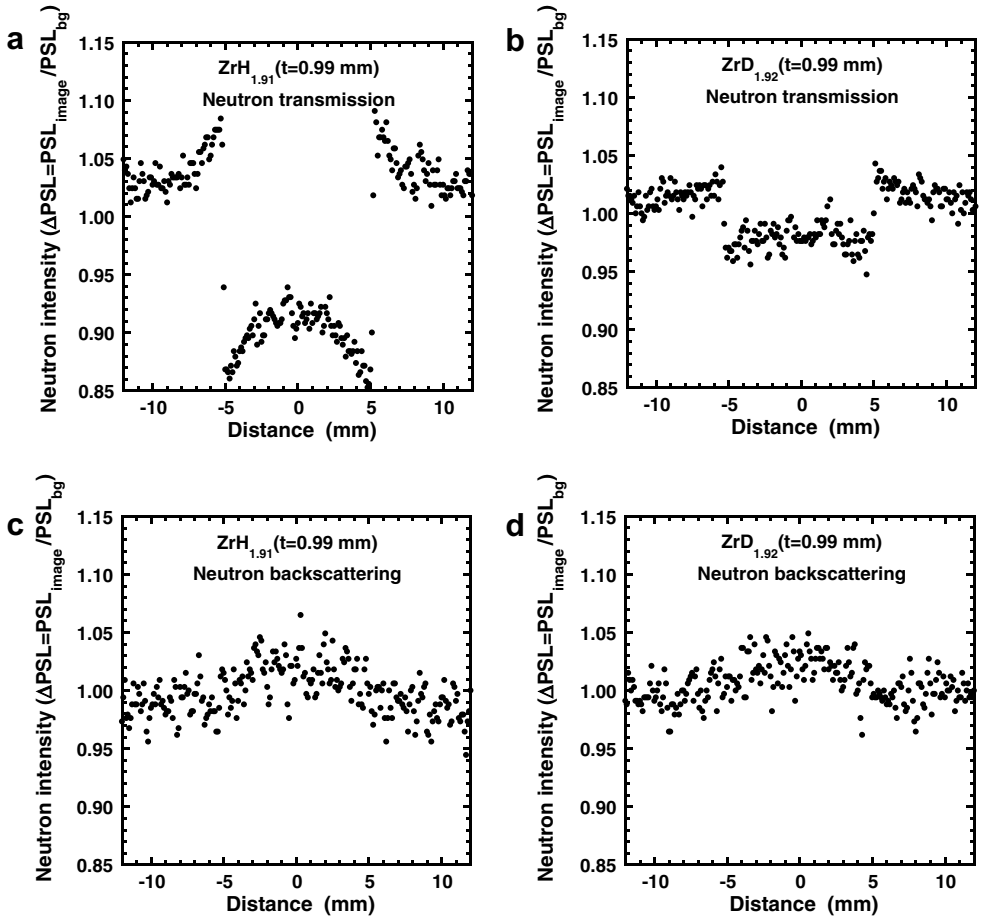

Fig. 3. ΔPSL values of transverse line profiles of the NRG transmission and backscattering images in Fig. 2.

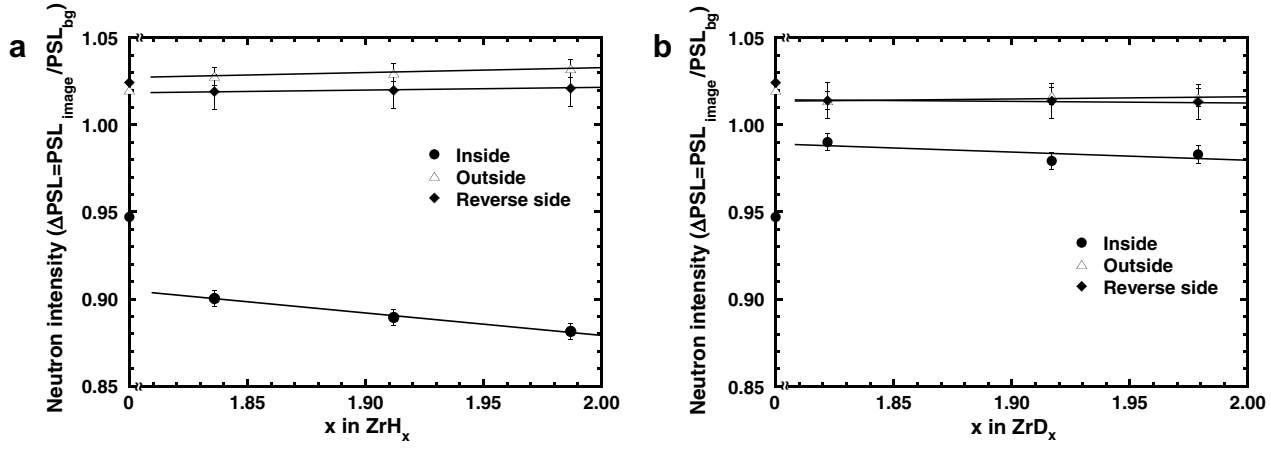

Fig. 4. ΔPSL values on the imaging plates at several parts of the inside, outside and reverse side for (a) ZrH_x and (b) ZrD_x.

hydrogen atoms can therefore be described by first-order reaction kinetics. The relationship between the PSL_{image} and PSL_{bg} for the transmission images can be expressed with the following equation:

$$PSL_{image} = PSL_{bg}\exp(-\mu t) \quad (1)$$

$$\mu = -\frac{1}{t}\ln(\Delta PSL) \quad (2)$$

where μ and t are thermal neutron linear attenuation coefficient [mm^{-1}] and specimen thickness [mm], respectively. Fig. 5 shows thermal neutron mass attenuation coefficients μ^{ZrH_x}/ρ^{ZrH_x}, μ^{ZrD_x}/ρ^{ZrD_x} and μ^{Zr}/ρ^{Zr} against H/Zr and D/Zr ratios, calculated by substituting the mean inside ΔPSL values of Fig. 4(a) and (b) and the specimen thickness to Eq. (2) and using the densities of ZrH_x, ZrD_x and Zr (ρ^{ZrH_x}, ρ^{ZrD_x} and ρ^{Zr}) which have been reported in the Refs.

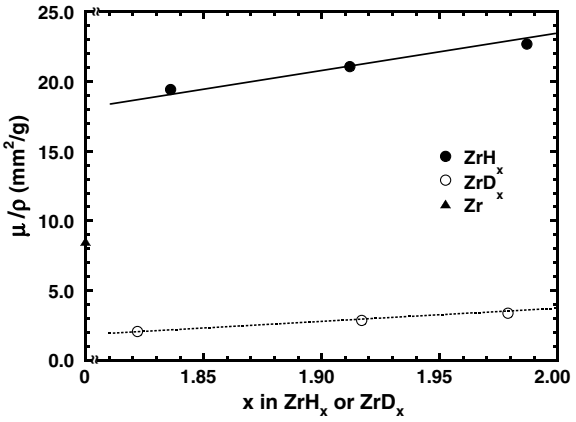

Fig. 5. Thermal neutron mass attenuation coefficients against hydrogen isotope concentrations in ZrH_x and ZrD_x.

[15,16]. The hydrogen concentration dependence of μ^{ZrH_x}, μ^{ZrD_x}, μ^{Zr}, $\rho^{ZrH_x}, \rho^{ZrD_x}$ and ρ^{Zr} for ZrH_x, ZrD_x and Zr can be expressed with empirical equations as a function of the ε-phase hydrogen concentration x ($1.7 < x < 2.0$) as follows: $\mu^{ZrH_x} = -0.108 + 0.118x$, $\mu^{ZrD_x} = -0.074 + 0.047x$, $\mu^{Zr} = 0.054$ [mm^{-1}], $\rho^{ZrH_x} = 1/(0.171 + 0.0042x)$, $\rho^{ZrD_x} = 1/(0.1745 + 0.0015x)$ and $\rho^{Zr} = 6.4$ [10^{-3} g/mm^3]. The value of μ^{ZrD_x}/ρ^{ZrD_x} for $1.8 < x < 2.0$ is about 1/6–1/9 and 1/2–1/4 times, respectively, as those of μ^{ZrH_x}/ρ^{ZrH_x} and μ^{Zr}/ρ^{Zr}.

3.3. Analyses of thermal neutron transmission and backscattering processes using MCNP calculation

The neutron scattering process for the NRG measurement was simulated by MCNP code [11] using the Japanese Evaluated Nuclear Data Library (JENDL) [14]. A track length tally estimator was used for the neutron intensity. Fig. 6(a)–(d) show the MCNP results of the neutron transmission and backscattering for specimens with H/Zr and D/Zr ratios 1.7, 1.8, 1.9, 2.0 and dimension of $\phi 10 \times 1$ mm^3. The data for Zr is also included in Fig. 6(a)–(d). Thermal neutrons with the energy of 0.0253 eV, and flat distribution of 20 mm in diameter, enter the specimen. The statistical error was less than 0.6%. The horizontal and vertical axes respectively represent the distance from the center of the specimen and the neutron intensity on the imaging plate. The transmission neutron intensity at the center of inside Zr is lower than the background, indicating absorption of neutrons by Zr nuclei. The neutron intensity at the edge of the inside is lower than that at

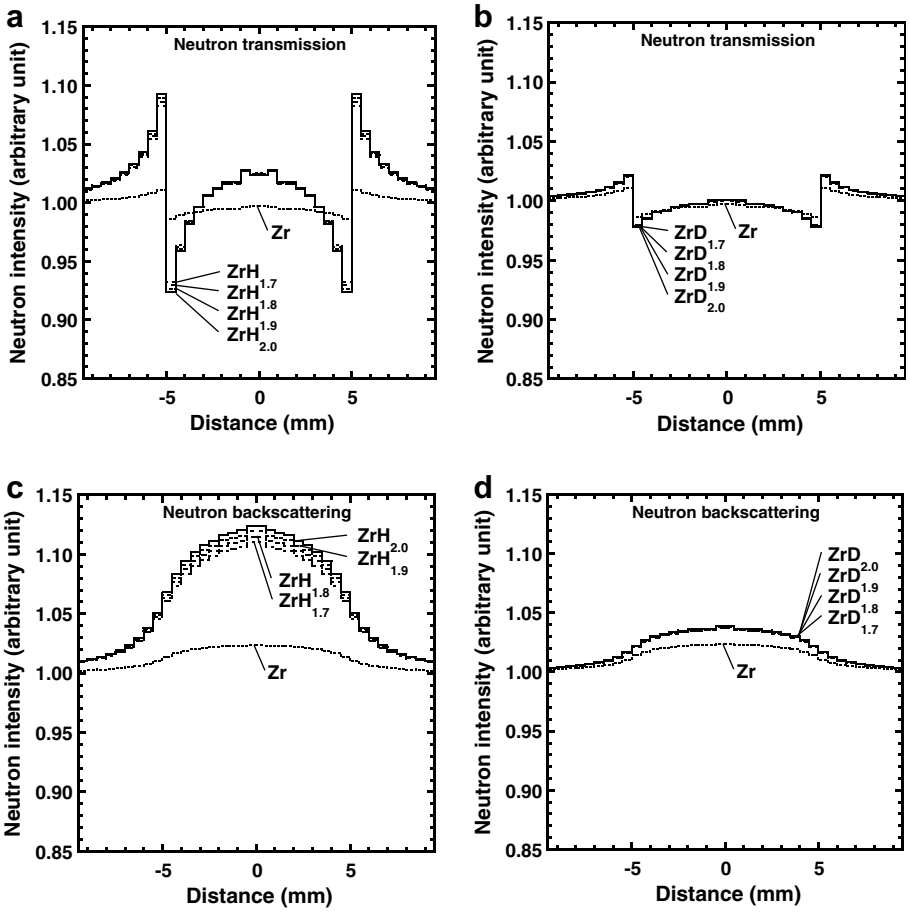

Fig. 6. Hydrogen isotope concentration dependence of thermal neutron transmission ((a) ZrH_x and (b) ZrD_x) and backscattering ((c) ZrH_x and (d) ZrD_x), calculated using MCNP code.

the center. The intensities at the outside and reverse side are higher than the background. In ZrH_x, the intensities at the outside and reverse side (or inside) increase (or decrease) as the hydrogen concentration increases. However, it is unable to see the hydrogen concentration dependence on the neutron scattering for ZrD_x. These calculation results are in agreement with the experimental results for the scattering processes and the isotope effects, although the absolute values are different. Hydrogen analysis by combining NRG experiments with MCNP calculations has potential application to evaluating protium redistribution in actinide hydride targets. However, to provide evidence of the efficiency of the method, it is clearly necessary to obtain more sensitive NRG images for protium as well as deuterium and to develop new NRG systems using cold neutrons with a single energy from a reactor or neutron source.

4. Summary

The forward-scattering and back-scattering of thermal neutrons in respect of hydrogen isotope concentrations in ε-ZrH_x and ε-ZrD_x ($1.8 < x < 2.0$) were studied by NRG at room temperature with a thermal neutron flux of 1.2×10^{12} n/m^2/s from the JRR-3M reactor at JAEA. The thermal neutron mass neutron attenuation coefficients for ZrH_x and ZrD_x were determined from the transmission NRG images. Isotope effects were observed, in that the thermal neutron mass attenuation coefficients for ZrH_x were about 6–9 times higher than those for ZrD_x. For the thermal neutron backscattering process, there were also hydrogen concentration dependence and isotope effects. The isotope effects in the thermal neutron transmission and backscattering processes were analyzed by MCNP calculation, in which the elastic and capture cross sections of thermal neutron to protium, deuterium and zirconium atoms were taken into account in thermal neutron scattering in zirconium hydrides and deuterides. The calculation results were similar to the experimental results for the scattering processes and the isotope effects. However, the absolute values are different, and moreover it proved impossible to estimate the deuterium concentrations of D/Zr = 1.7–2.0 for the thermal neutron-transmitted and -backscattered NRG images, since the elastic cross section of deuterium is about 1/3 times that of zirconium. It is therefore necessary to modify considerably the method by combining NRG experiments with MCNP calculations to be able to apply it as non-destructive hydrogen analysis for PIE experiments.

Acknowledgments

The authors thank Dr. H. Andou and Dr. M. Nakata for the NRG results. This work was supported by the Japan Atomic Energy Agency.

References

[1] K. Konashi, B. Tsuchiya, M. Yamawaki, K. Fujimura, T. Sanda, Development of actinide-hydride targets for transmutation of nuclear waste, in: International Conference on Back-End of the Fuel Cycle from Research to Solutions, GLOBAL2001, Paris France, 9/13 September, 2001.
[2] J. Huang, B. Tsuchiya, K. Konashi, M. Yamawaki, J. Nucl. Sci. Technol. 37 (10) (2000) 887.
[3] J.S. Cantrell, R.C. Bowman Jr., D.B. Sullenger, J. Phys. Chem. 88 (1984) 918.
[4] S.E. Kul'kova, O.N. Muryzhnikova, Int. J. Hydrogen Energy 24 (1999) 207.
[5] B. Tsuchiya, M. Teshigawara, K. Konashi, M. Yamawaki, J. Alloy Compd. 330–332 (2002) 357.
[6] P.W. Bickel, T.G. Berlincourt, Phys. Rev. B 2 (1970) 4807.
[7] K.G. Barraclough, C.J. Beevers, J. Nucl. Mater. 34 (1970) 125.
[8] M. Zanarini, P. Chirco, M. Rossi, G. Guidi, E. Querzola, M.G. Scannavini, F. Casali, A. Garagnani, A. Festinesi, IEEE Trans. Nucl. Sci. 42 (1995) 580.
[9] H. Sakaguchi, A. Kohzai, K. Hatakeyama, S. Fujine, K. Yoneda, K. Kanda, T. Esaka, Int. J. Hydrogen Energy 25 (2000) 1205.
[10] B. Tsuchiya, M. Teshigawara, S. Nagata, K. Konashi, R. Yasuda, Y. Nishino, T. Nakagawa, M. Yamawaki, Nucl. Instrum. and Meth. B 190 (2002) 699.
[11] MCNP-A General Monte Carlo N-Particle Transport Code, LA-12625-M (Rev.) Version 4B, Transport Methods Group, Los Alamos National Laboratory, 1997.
[12] B. Tsuchiya, J. Huang, K. Konashi, M. Teshigawara, M. Yamawaki, J. Nucl. Mater. 289 (2001) 329.
[13] N. Niimura, Y. Karasawa, I. Tanaka, et al., Nucl. Instrum. and Meth. A 349 (1994) 521.
[14] T. Nakagawa, S. Shibata, S. Chiba, T. Fukahori, Y. Nakajima, Y. Kikuchi, T. Kawano, Y. Kanda, T. Ohsawa, H. Matsunobu, M. Kawai, A. Zukeran, T. Watanabe, S. Igarashi, K. Kosako, T. Asami, J. Nucl. Sci. Technol. 32 (12) (1995) 1259.
[15] M.T. Simnad, Nucl. Eng. Des. 64 (1981) 403.
[16] B. Tsuchiya, M. Teshigawara, K. Konashi, S. Nagata, T. Shikama, M. Yamawaki, J. Nucl. Sci. Technol. 39 (4) (2002) 402.